AFRL-AFOSR-JP-TR-2022-0032

Study of non-equilibrium wakes model

McIntyre, Timothy
THE UNIVERSITY OF QUEENSLAND
UNIVERSITY OF QUEENSLAND
BRISBANE, , 4072
AUS

05/24/2022
Final Technical Report

Air Force Research Laboratory
Air Force Office of Scientific Research
Asian Office of Aerospace Research and Development
Unit 45002, APO AP 96338-5002

REPORT DOCUMENTATION PAGE

PLEASE DO NOT RETURN YOUR FORM TO THE ABOVE ORGANIZATION.

1. REPORT DATE	2. REPORT TYPE	3. DATES COVERED	
20220524	Final	START DATE 20190218	END DATE 20220217

4. TITLE AND SUBTITLE
Study of non-equilibrium wakes model

5a. CONTRACT NUMBER	5b. GRANT NUMBER	5c. PROGRAM ELEMENT NUMBER
	FA2386-19-1-0012	61102F
5d. PROJECT NUMBER	**5e. TASK NUMBER**	**5f. WORK UNIT NUMBER**

6. AUTHOR(S)
Timothy McIntyre

7. PERFORMING ORGANIZATION NAME(S) AND ADDRESS(ES)
THE UNIVERSITY OF QUEENSLAND
UNIVERSITY OF QUEENSLAND
BRISBANE 4072
AUS

8. PERFORMING ORGANIZATION REPORT NUMBER

9. SPONSORING/MONITORING AGENCY NAME(S) AND ADDRESS(ES)	10. SPONSOR/MONITOR'S ACRONYM(S)	11. SPONSOR/MONITOR'S REPORT NUMBER(S)
AOARD UNIT 45002 APO AP 96338-5002	AFRL/AFOSR IOA	AFRL-AFOSR-JP-TR-2022-0032

12. DISTRIBUTION/AVAILABILITY STATEMENT
A Distribution Unlimited: PB Public Release

13. SUPPLEMENTARY NOTES

14. ABSTRACT
Fundamental ground-based experiments were conducted to investigate radiation produced in the wake of a hypersonic vehicle operating with a heated ablative forebody. Two simple model configurations were investigated - a double compression (double wedge) followed by an expansion, and a single compression (wedge) followed by an expansion. Each model was designed so that a plate could be inserted into the leading surface to facilitate ablation. Plates consisting of unheated aluminium, unheated/heated graphite, and unheated/heated carbon-carbon were investigated. Spectroscopy and high-speed imaging were conducted in each experiment, and calibrated spectral
radiances were obtained at multiple locations and over multiple wavelength ranges. The results indicated that ablative products entered the flow when using a heated carbon-carbon plate. This was inferred by the presence of the CN molecule which was detected in flow near the compression surface downstream of the plate (double wedge and single wedge) and in the expansion region beyond the body (single wedge). The tests (70 in total) provide an important database for comparison with current and future numerical simulations of the flow.

15. SUBJECT TERMS

16. SECURITY CLASSIFICATION OF:			17. LIMITATION OF ABSTRACT	18. NUMBER OF PAGES
a. REPORT U	b. ABSTRACT U	c. THIS PAGE U	SAR	21

19a. NAME OF RESPONSIBLE PERSON	19b. PHONE NUMBER *(Include area code)*
RYAN CARR	315-227-7005

Award Number: FA2386-19-1-0012

Report Type: Final Performance Report

Principal Investigator: Professor Timothy McIntyre

Principal Investigator Email: t.mcintyre@uq.edu.au

Principal Investigator Phone: +61 403 123 242

Project Title: Study of Non-Equilibrium Wakes Model

Recipient Organization: The University of Queensland

Business Office Email: internationalgrants@research.uq.edu.au

Report Due Date: 18 May 2022

Reporting Period Start Date: 18 February 2019

Reporting Period End Date: 17 February 2022

Program Officer: Lt Col Ryan W. Carr, PhD, USAF

1 Accomplishments

1.1 Research Objectives

The primary objectives of this proposal (as described in the project narrative) were to

- Perform measurements in the University of Queensland X2 expansion tube in which ablative products were introduced into the flow from a hot and ablating upstream thermal protection system (TPS) material mounted on a test model
- Use surface materials that are representative of TPS materials of interest to USAF, and reference benchmark materials such as graphite and metallic surfaces.
- Obtain experimental data in the form of calibrated spectral measurements made from within the upstream flow regions and the wake in the ultraviolet to mid infrared spectral regions.
- Conduct experiments (70 tests) that aimed to cover broad parametric space, with variations in wall temperature, materials, flow enthalpy, length scale and flow compression and expansion factors adjusted in consultation with AFIT.
- Use the results of the experiments to evaluate the validity of current theoretical and numerical methods used to model the radiation from hypersonic wakes.

1.2 Accomplishments during this reporting period

Over the course of the project, all of the above objectives have been met to varying levels. Specifically

- A total of 70 tests have been performed in the X2 facility. These tests have covered two model configurations: a double-compression wedge followed by an expansion, and a simpler single compression followed by an expansion. There were some changes from the originally proposed configurations. These changes are discussed in the relevant section below.
- Testing was conducted using an AFIT-supplied carbon-carbon ablator at various temperatures, a graphite ablator, and a cold aluminium surface.
- Spectroscopic measurements were obtained at ultraviolet, visible and near-infrared wavelengths both downstream of the ablator as well as in the expansion region downstream of the test model.
- Comparisons were made (by our AFIT collaborators) between the experimental measurements and numerical simulations of the flow configurations. These comparisons are ongoing.

Under the revised approach approved by the grantor, all goals have been met and a valuable database of experimental measurements has been created.

1.3 Dissemination

The work has thus far been disseminated by a number of avenues and publications:

Journal articles

- MacDermott, R., Greendyke, R., Temme, N., Morgan, R., and McIntyre, T., *Experimental Analysis of Hypersonic Carbon-Carbon Ablation in Representative-Wake Expansion Regions*, JANNAF Journal of Propulsion and Energetics, Vol 12, Issue 1, 2021.
- (Submitted) MacDermott, R., Temme, N., Morgan, R., and McIntyre, T., *Computational Analysis of Hypersonic Carbon-Carbon Ablation in Representative-Wake Expansion Regions*, JANNAF Journal of Propulsion and Energetics, 2022.

Conference papers with presentations

- MacDermott, R., and Greendyke, R., *Experimental Analysis of Gas-Surface Interactions with Ablating Material*, 2020 National Space and Missile Materials Symposium, Virtual Meeting, June 2020.
- MacDermott, R., Greendyke, R., Temme, N., Morgan, R., and McIntyre, T., *Experimental Analysis of Hypersonic Carbon-Carbon Ablation in Representative-Wake Expansion Regions*, 38th Exhaust Plume and Signatures Meeting (JANNAF), 2020-0006N, Virtual Meeting, December 2020.
- MacDermott, R., Temme, N., Morgan, R., and McIntyre, T., *Computational Analysis of Hypersonic Carbon-Carbon Ablation in Representative-Wake Expansion Regions*, 39th Exhaust Plume and Signatures Meeting (JANNAF), Norfolk, VA, June 2021.

Conference presentations

- MacDermott, R., Greendyke, R., Temme, N., Morgan, R., and McIntyre, T., *Experimental Analysis of Hypersonic Carbon-Carbon Ablation in Representative-Wake Expansion Regions* 2021 National Space and Missile Materials Symposium, Virtual Meeting, June 2021.
- McIntyre, T.J., Temme, N, Morgan, R.J., MacDermott, R., *Study of Non-Equilibrium Wakes Model*, 2021 AFOSR/HVSI/ONR High-Speed Aerodynamics Annual Review, July 19-23, 2021.
- MacDermott, R., Greendyke, R., Temme, N., Morgan, R., and McIntyre, T., *Experimental Analysis of Hypersonic Carbon-Carbon Ablation in Representative-Wake Expansion Regions*, 2021 Hypersonic Technology and Systems Conference, Virtual Meeting, October 2021.

Theses/Dissertations

- MacDermott, Robert B., *Experimental and Computational Investigation of Radiating Gas in Hypersonic Wakes*, Air Force Institute of Technology, AFIT-ENY-DS-21-S-099, September 2021.

- (submitted) Temme, Nils, *Hypervelocity boundary-layer flow experiments with high surface temperature ablation*, The University of Queensland, 2021.

Several further journal publications are planned relating to the experimental campaign on the second (simpler) configuration.

2 Impacts

The major outcome of this work is the dataset of experimental measurements. These consist of fully calibrated spectroscopic images of flow in the test facility. The database consists of

- One consistent flow condition with a nominal free-stream flow speed of 7.5 km/s and a flow enthalpy of around 30 MJ/kg
- Two model configurations (single wedge, double wedge) each with an ablating plate and subsequent expansion
- Ablating plates made from a carbon-carbon material, from graphite and for room-temperature aluminium
- Ablating plate temperatures from room temperature to around 2300 K
- High speed flow luminosity imaging with side and top views
- Spectroscopic measurements at wavelengths ranging from 350 nm to 1550 nm

This set of measurements is available to other researchers to access to test numerical simulations of these complex reacting flow fields. Such an extensive dataset of ablative measurements in a high-speed facility has not previously been available to the research community.

The project has enhanced the research relationship between the University of Queensland and the Air Force Institute of Technology. The first experimental campaign (in January 2020) involved a personnel exchange with LtCol Robert MacDermott (AFIT) visiting and working with Mr Nils Temme (UQ) and Prof Tim McIntyre (UQ). LtCol MacDermott was able to assist with the first experimental campaign as well as deliver the carbon-carbon plates used in this and the subsequent campaign. Although further visitations were not possible, the research team continued to have regular (weekly/fortnightly) meetings over Zoom to work collaboratively on the project. The team has since investigated options for further funding and plan to continue the collaborative research already performed. The synergy between UQ (experimental facilities) and AFIT (numerical capabilities) will be particularly beneficial in future projects.

A further pleasing outcome of the research is the completion of two PhD theses by postgraduate students who participated in the project. Mr Nils Temme (UQ) performed the experimental measurements on the X2 facility and some of the research performed formed part of his PhD dissertation which has been submitted for review. Likewise, LtCol Robert MacDermott (AFIT), who performed numerical simulations as part of the project, was able to complete and submit his dissertation which has since seen him successfully graduate with a PhD.

A number of other research higher degree students were involved in the experimental campaigns. Although the work performed by these students did not directly form part of their research project, the experiences gained in participating in the study were highly beneficial in furthering their own experimental abilities.

3 Changes

The project began in 2019 and the first experimental campaign (22 tests) was conducted early in 2020. As noted earlier, LtCol Robert MacDermott was able to travel to Australia to deliver the carbon-carbon ablating plates and to participate in this experimental campaign. However, Covid-19 began impacting on all aspects of life in March 2020, and Australia entered a nation-wide shutdown on 23 March 2020. This shutdown continued for some months and further restrictions and brief shutdowns continued until the end of 2021. Australian international borders remained closed over an extended period and it has only recently become possible for researchers to travel into and out of Australia. These disruptions have had a significant impact on the progress of the project as discussed in the sections below.

3.1 Changes in approach

The initial proposal for the project was to perform measurements on both two-dimensional and axisymmetric configurations. Flat ablating plates were designed and manufactured prior to the pandemic and hence two-dimensional testing was able to be performed. Axisymmetric testing was planned for the second half of the campaign but this approach was discarded (in consultation with the agency) as it became obvious that the manufacture and delivery (from the US) of plates suitable for axisymmetric testing would not be feasible. It was hence decided that the experimental campaign using two-dimensional models would be expanded, especially after examining the results from the initial campaign which indicated that a simpler two-dimensional model would be more suitable for comparisons with numerical simulations.

3.2 Problems or delays

Delays in the project occurred for several main reasons:

- Personnel. UQ staff participating in the project (including the project lead) are mostly teaching and research academics. All teaching activities continued during the pandemic but it was necessary for staff to devise and implement new online approaches to teaching. There was a significant added workload involved in this process, and hence a limitation on available time for research.
- Travel. LtCol Robert MacDermott was unable to visit and participate in further campaigns due to the restrictions on international travel. UQ personnel were unable to complete planned visits to AFIT.
- Facility access. All experimental campaigns in the X2 facility were impacted by the shutdowns, by the reduced access to resources (limited deliveries), and the general day-to-day impact on life. These delays saw the planned second experimental campaign deferred by around 1-year, the eventual approved extension time for the project.

3.3 Expenditure Impacts

There were no overall changes in the project expenditure. However, on approval, funding initially allocated for international travel was re-purposed to address the personnel issue. A research assistant (Mr Nils Temme) was appointed to perform the second campaign and subsequent analysis.

4 Technical Updates

This section provides a commentary to the datasets that were obtained during the program. It covers the key outcomes identified during the project. Analysis is ongoing and further outcomes will be published when this analysis is complete.

Abstract

Fundamental ground-based experiments were conducted to investigate radiation produced in the wake of a hypersonic vehicle operating with a heated ablative forebody. Two simple model configurations were investigated - a double compression (double wedge) followed by an expansion, and a single compression (wedge) followed by an expansion. Each model was designed so that a plate could be inserted into the leading surface to facilitate ablation. Plates consisting of unheated aluminium, unheated/heated graphite, and unheated/heated carbon-carbon were investigated. Spectroscopy and high-speed imaging were conducted in each experiment, and calibrated spectral radiances were obtained at multiple locations and over multiple wavelength ranges. The results indicated that ablative products entered the flow when using a heated carbon-carbon plate. This was inferred by the presence of the CN molecule which was detected in flow near the compression surface downstream of the plate (double wedge and single wedge) and in the expansion region beyond the body (single wedge). The tests (70 in total) provide an important database for comparison with current and future numerical simulations of the flow.

4.1 Experimental facility and diagnostics

All measurements were conducted in the X2 expansion tube at the University of Queensland. A schematic diagram of the facility is shown in Fig. 1.

A free-piston is used to compress and heat a helium driver gas. On rupture of the primary diaphragm, a shock wave propagates through the test gas (air), initially in the shock tube, which is compressed and accelerated. This shock ruptures the secondary diaphragm and the test gas expands into the acceleration tube and through the nozzle, entering the test section. Further details can be found about the operation of the facility in [1].

All tests were conducted using a single operating condition with a total enthalpy of 31.4 MJ/kg, corresponding to an equivalent flight speed of about 7.9 km/s. The nominal free-stream conditions in the test gas are shown in Table 1. Dissociation levels in the free-stream are negligible. There were some small shot-to-shot variations.

Tests were performed using two models, each designed with a compression and expansion region. In the compression region, a replaceable insert was designed that could be electrically heated prior to each test. The inserts were plates of three different materials: aluminium (unheated), graphite, and an aerospace grade carbon-carbon (C-C) material.

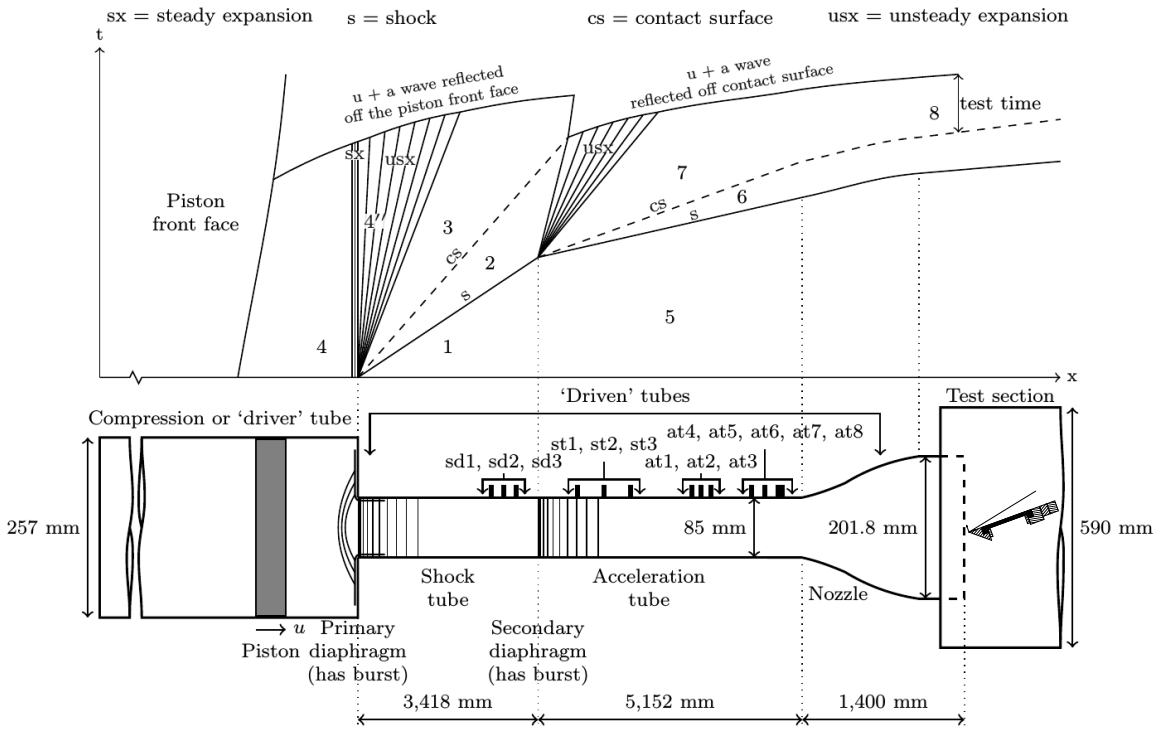

Figure 1: Schematic diagram of the X2 expansion tube.

The latter was supplied by our collaborator, Robert MacDermott from the Air Force Institute of Technology.

The flow in each test was viewed using a range of optical instruments including high-speed cameras imaging the integrated flow luminosity and spectrometers instrumented with intensified cameras. Figure 2 shows the configuration used in the second campaign (a similar experimental approach was used in the first campaign). The spectroscopic measurements were recorded with three separate spectrometer/camera systems. A PI-Max 4 intensified CCD camera coupled to an Acton SpectraPro-2300i spectrometer was used to record spectra in the compression region of the flow. Similarly an Andor iStar 340T intensified camera also coupled to an Acton SpectraPro-2300i spectrometer was used to observe the expansion region. Lastly, an IRC 806 infrared camera coupled with a Acton SpectraPro-2500i was used to also view the expansion region. A Phantom high-speed camera was used to observe the flow from the side, while a Shimadzu high-speed camera observed the flow from above. The temperature of the inserted plate, when heated, was determined using a camera system which was used to record images of the plates through filters at different wavelength regions. Further details of all the diagnostic systems can be found in [3].

4.2 Test Model 1 - Results and analysis

The test model used in the first campaign is shown in Fig. 3. It consisted of an adjustable double-wedge followed by compression and expansion surfaces. Figure 3(a) shows a side on schematic of the model. The wedge was placed at an angle of 20° to the incoming flow with the second compression stage providing a further 20° increase in angle. The expansion stage then had an opening angle of 45°. The width of the model was 90 mm. The red vertical lines in the figure show the locations of the spectral measurements conducted in

Table 1: Operating conditions for all tests

Parameter	Value
Total enthalpy	31.4 MJ/kg
Velocity	7.43 km/s
Equivalent flight velocity	7.92 km/s
Density	0.0219 kg/m^3
Temperature	2880 K
Mach number	7.46
Reynolds number	1.8x10^6 /m

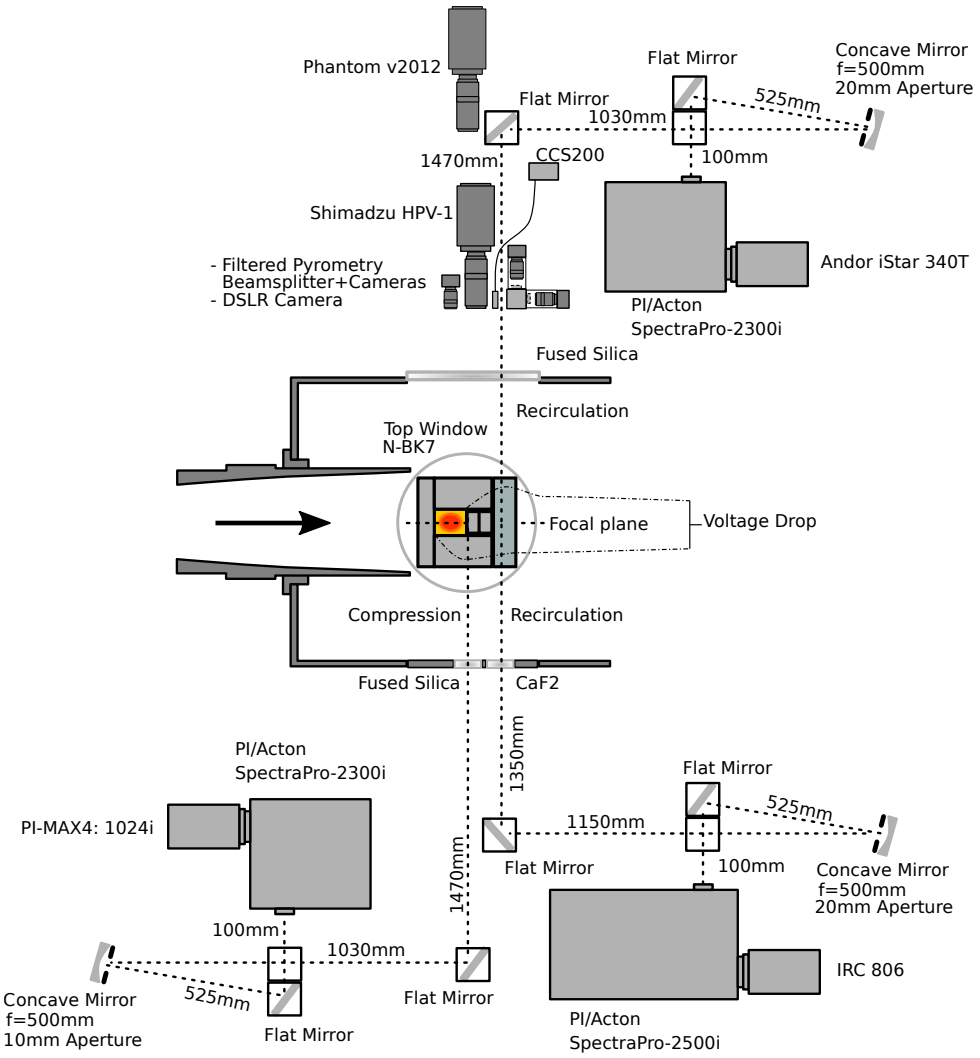

Figure 2: Optical configuration for performing measurements.

these tests, the first being just downstream of the heated plate, and the second in the expansion region. Figure 3(b) shows a photo of the model. The 50 mm by 50 mm heated plate that is inserted in the surface of the wedge is evident in the image.

A high-speed image of the flow luminosity, superimposed on a diagram of the model, is shown in Fig. 4. It shows shock waves generated from the leading edge of the model and from the second compression. A brighter viscous layer near the surface of the model

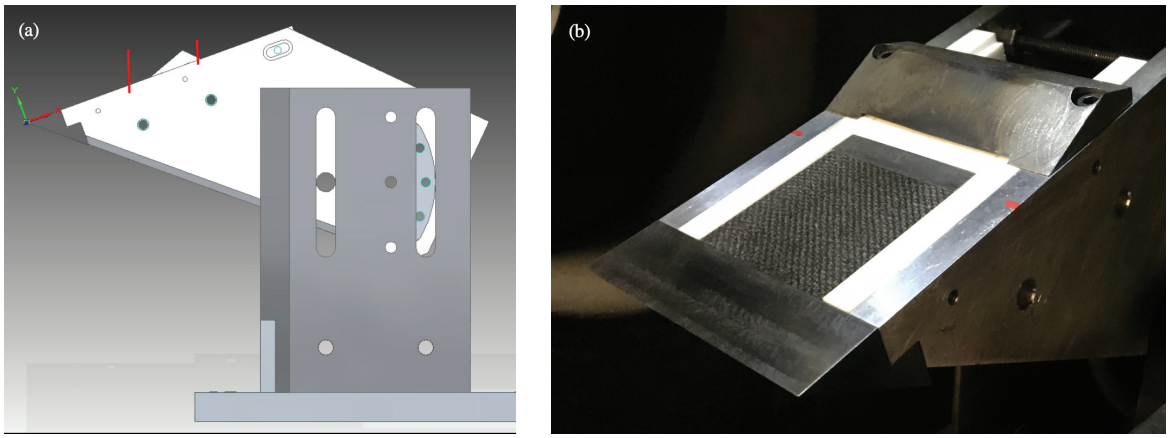

Figure 3: Model 1 - configuration used in testing. (a) Model schematic; (b) Photo.

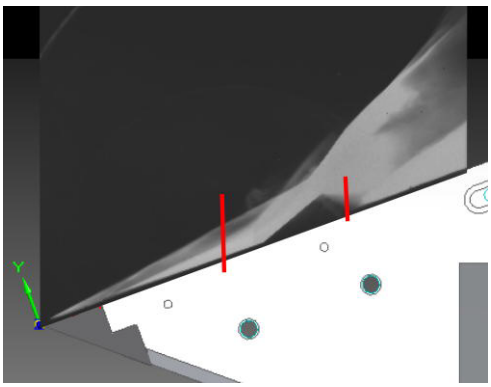

Figure 4: Model 1 - high-speed image of the flow. Red lines indicate locations for spectroscopy.

which continues above the expansion region is also evident. Red lines again show the locations at which spectroscopic measurements were recorded.

Table 2: Analysed tests for Model 1

X2 Test	Label	Plate material	Temperature
4595	Al	Al	Unheated
4596	Al	Al	Unheated
4599	Al	Al	Unheated
4590	CC-Cold	C-C	Unheated
4591	CC-Cold	C-C	Unheated
4584	CC-1000	C-C	1000 K
4585	CC-1300	C-C	1300 K
4588	CC-1560	C-C	1560 K
4602	CC-2000	C-C	2000 K
4594	CC-2000	C-C	2000 K
4603	CC-2300	C-C	2300 K

A total of 34 tests were conducted using this model over two campaigns (January 2020 and November 2021). Included in these tests were 11 heated C-C tests and one

heated graphite test. Cold tests were also completed with aluminium, graphite and C-C plates. A matrix of tests that were analysed in detail is given in Table 2. These tests were performed with a coarser diffraction grating in each spectrometer (150 lines per mm) than later tests to allow broad spectral regions to be viewed in each test. A full list of tests can be found in the appendix.

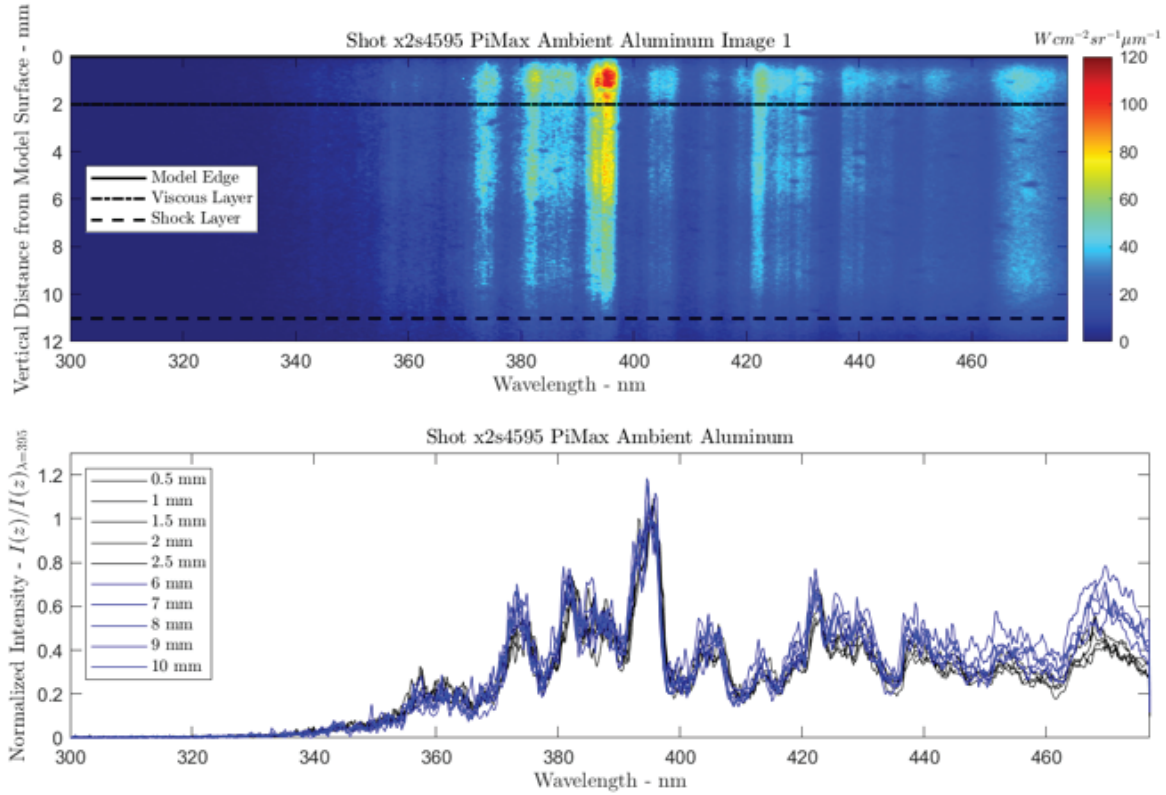

Figure 5: Example spectra from test 4595 (aluminium), compression region. Upper: Full calibrated image; Lower: selected spectra. Credit: R. MacDermott

Figure 5 shows an example spectroscopic image recorded in an X2 test with an unheated aluminium plate. The upper image shows a two-dimensional colour map that is recorded on the camera. Initially the horizontal and vertical axes are pixel number while the colour axis is camera counts. Each axis is calibrated through separate processes:

- The horizontal axis is converted to wavelength. This is achieved by either recording an image of a spectral lamp with known spectral lines and then converting pixel number to wavelength. Alternatively, self-calibration is possible by identifying prominent lines of contaminants in the flow (chiefly iron).
- The vertical axis is converted to position above the plate. This is achieved by recording an image of a calibration plate illuminated by a lamp. By viewing markers of known location in the image, pixel number is converted to position.
- The colour axis is converted to spectral radiance (in units of $\mathrm{Wcm^{-2}sr^{-1}\mu m^{-1}}$) by recording an image of a calibration lamp (Labsphere CSTM-USS-400-HI spectral radiance source) placed in the test section of the facility and imaged using the same optical system as used in an X2 test. The lamp is provided with a known spectral

radiance for wavelengths between 300 nm and 1000 nm, and thus a wavelength-dependent calibration factor (spectral radiance per count) can be determined.

The outcomes of these calibrations can be seen in the upper plot of Fig. 5 with quantitative values for wavelength, position and spectral radiance all shown. Spectra can be extracted from these images by selecting a row of pixels and plotting the spectral radiance as a function of wavelength (normally some spatial averaging is performed by averaging over multiple rows). Such spectra, at various heights above the plate, are shown in the lower plot of Fig. 5. These have been normalised against the spectral radiance recorded at 395 nm in each image. The features evident is these plots are all related to flow contaminants, and most can be identified as being due to iron in the flow. Such contaminants are entrained into the test gas before it reaches the test section.

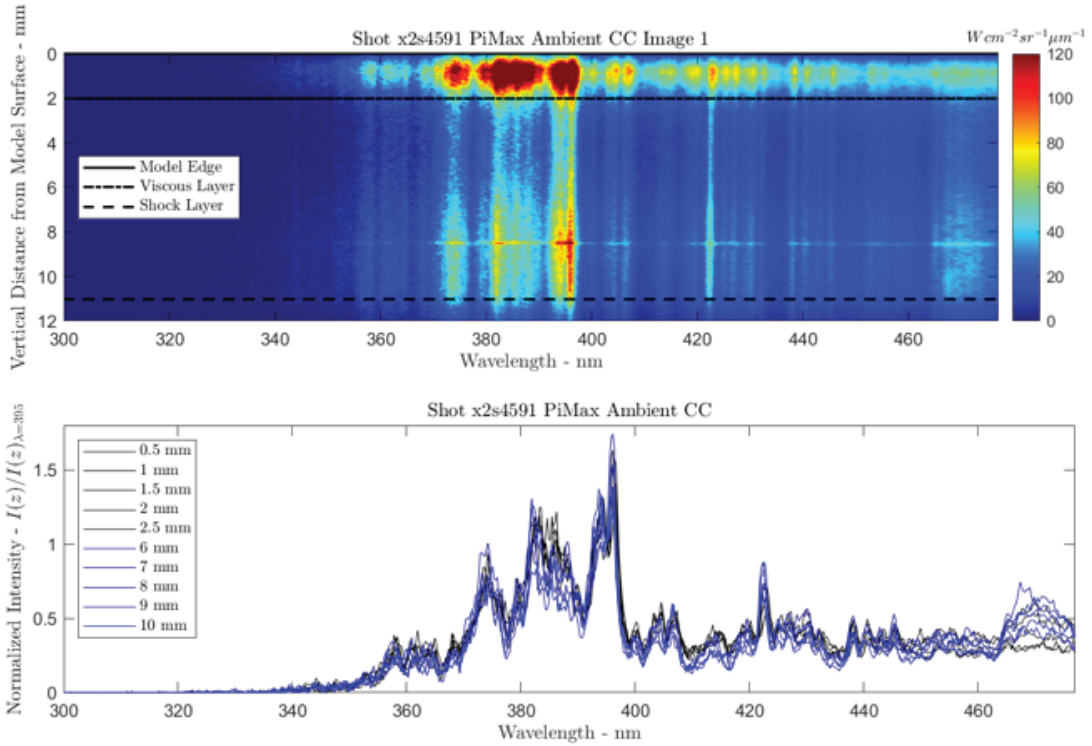

Figure 6: Example spectra from test 4591 (C-C cold), compression region. Upper: Full calibrated image; Lower: selected spectra. Credit: R. MacDermott.

Figure 6 shows a similar result for an unheated cold carbon-carbon plate. The spectral features are almost identical to the test with an aluminium plate.

In contrast, Fig. 7 shows the results for a heated C-C test. The recorded surface temperature of the plate immediately before the test was around 1250 K. There is evidently more signal in the wavelength range 380–390 nm within the viscous layer near the surface of the plate. Further from the plate, outside this viscous layer, a spectral distribution similar to the unheated test is observed. This brighter feature in the viscous layer can be identified as being due to the CN molecule (CN violet, Δv=0 bands). A similar (but weaker) feature is observed over the range 410-420 nm which can also be identified as being due to the CN molecule (CN violet, Δv=-1 bands).

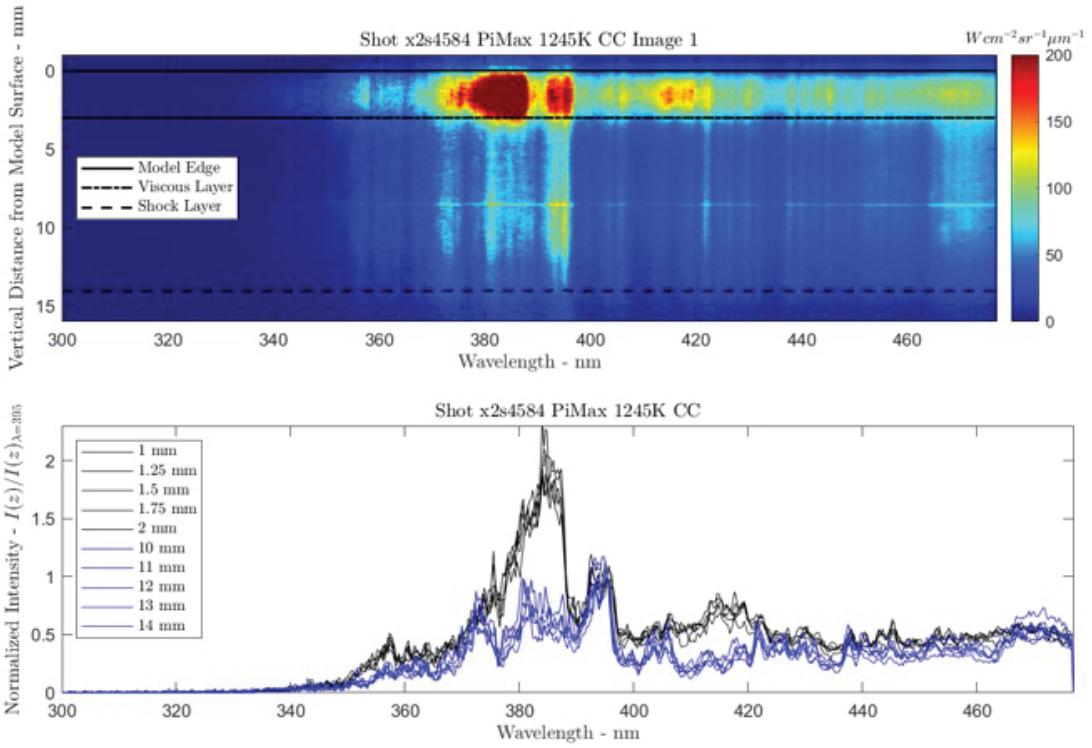

Figure 7: Example spectra from test 4584 (C-C hot), compression region. Upper: Full calibrated image; Lower: selected spectra. Credit: R. MacDermott.

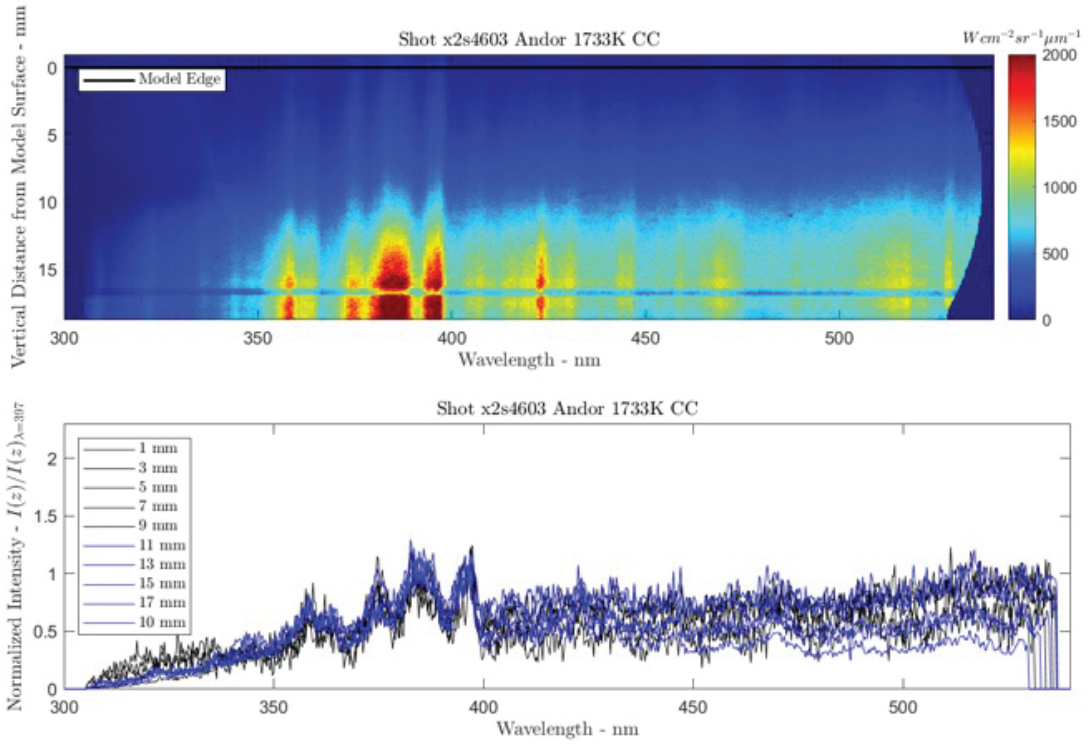

Figure 8: Example spectra from test 4603 (C-C hot), expansion region. Upper: Full calibrated image; Lower: selected spectra. Credit: R. MacDermott.

These spectra, observed only for heated carbon-carbon tests, provide firm evidence of the ablation and entrainment into the flow of carbon species from the heated plate during the test time. Carbon reacts with nitrogen in the test gas to form CN, a known bright radiator.

Figure 8 shows spectra recorded in the expansion region downstream of the step. Although this test was recorded with a heated plate, no species identified as being due to ablation from the plate were observed.

A more complete analysis of these tests, and some comparisons with numerical simulation, can be found in [4].

The results of this study indicated that a simpler configuration (single compression and expansion) would be preferable for comparison between experimental measurements and numerical simulations. Higher resolution spectra were also desired.

4.3 Test Model 2 - Results and analysis

The second campaign utilised a simpler single-compression, expansion configuration. This model is shown schematically in Fig. 9. The wedge had an angle of 20° to the free-stream and was similarly designed to allow heated plates to be inserted into the surface. Expansion was achieved by the use of a 90° step with a 10 mm step height. This model also had a width of 90 mm. The operating conditions for the facility were identical to the testing conducted with the first model.

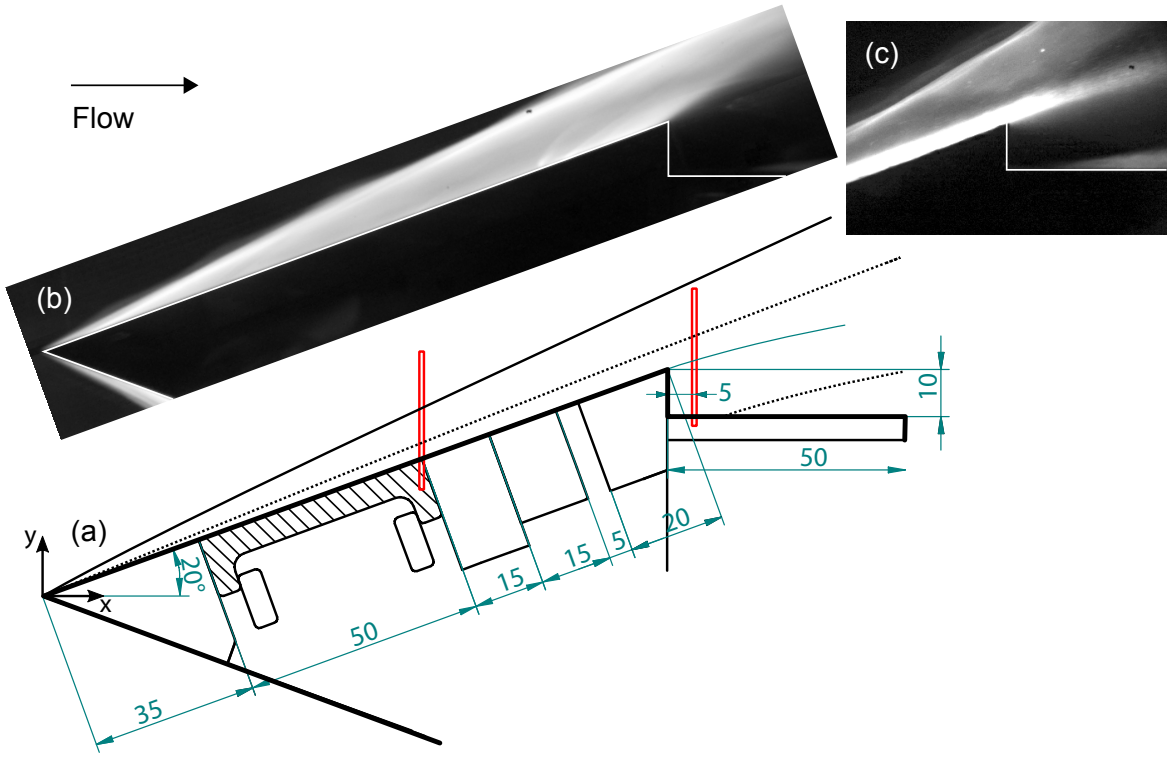

Figure 9: Model 2 - configuration used in testing. (a) Model schematic and dimensions (red lines indicate locations for spectroscopy); (b) Sample high speed image; (c) Sample (enhanced) high speed image of flow over the step.

The figure shows two example high-speed images that were recorded during testing. Some small disturbances are seen downstream of the plate. These result from the design

of the model which has a small gap to accommodate the thermal expansion of the inserted plates when heated. The two location where spectroscopic images were recorded are also shown.

Table 3: Analysed tests for Model 2

X2 Test	Label	Plate material	Current	Temperature
5011	Al	Al	-	Unheated
5020	CC-Cold	C-C	-	Unheated
5033	CC-600	C-C	600 A	1700 K
5032	CC-800	C-C	800 A	2000 K
5034	CC-1100	C-C	1100 A	2200 K
5031	G-1200	Graphite	1200 A	2300 K

The tests that were analysed in detail and presented in this report are shown in Table 3. Unheated tests with aluminium and carbon-carbon plates were analysed along with heated tests for carbon-carbon for various heating currents, and one heated graphite test. Results presented here are from the camera system viewing the flow downstream of the step over a wavelength range of 360-440 nm.

Figure 10 shows a sample image from this series of testing for a heated carbon-carbon insert. This is from the spectrometer imaging the flow downstream of the step. A higher

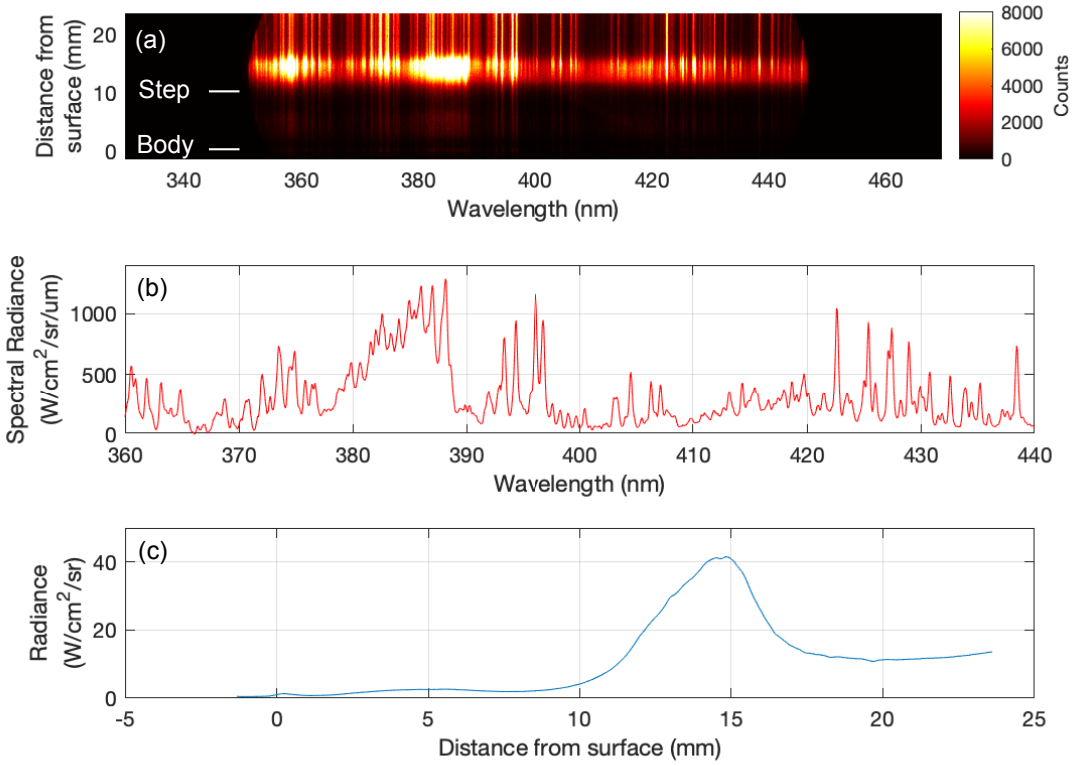

Figure 10: Example data from test 5034 (heated C-C), expansion region. (a) Full two-dimensional image; (b) Sample spectrum at peak intensity; (c) Radiance obtained by integrating over the wavelength range 360 – 440 nm.

resolution diffraction grating has been used in the spectrometer leading to more clearly resolved spectral lines than those presented for Model 1 (albeit at a cost of the range of wavelengths recorded in a single test).

Three different radiating regions are apparent in Figure 10(a). The first 10 mm above the surface is the region below the step and radiation levels are low. Between 10 mm and 15 mm is the brighter viscous flow region which was the flow from near the surface of the wedge. Above 15 mm is the flow behind the leading-edge oblique shock – the shock itself is above the top of the image. Figure 10(b) shows a calibrated spectrum from the brightest radiating layer at about 13 mm above the surface. Evident are a range of spectral lines along with the broader CN feature observed between 380 nm and 390 nm. In Figure 10(c), the spatial distribution of the radiation can be observed - brightest in the viscous layer and dimmest in the expansion region.

Figure 11 shows a spectrum from the viscous layer for a test with an unheated aluminium plate (over a narrower wavelength range). Superimposed on the left plot are calculated spectra for a range of different atomic species. Note that both the experimental spectrum and the calculated spectra are absolute – there has been no rescaling of respective spectral radiances. The calculations use input values of flow temperature, species concentration, spectral line broadening and instrument function. Optical thickness is also accounted for.

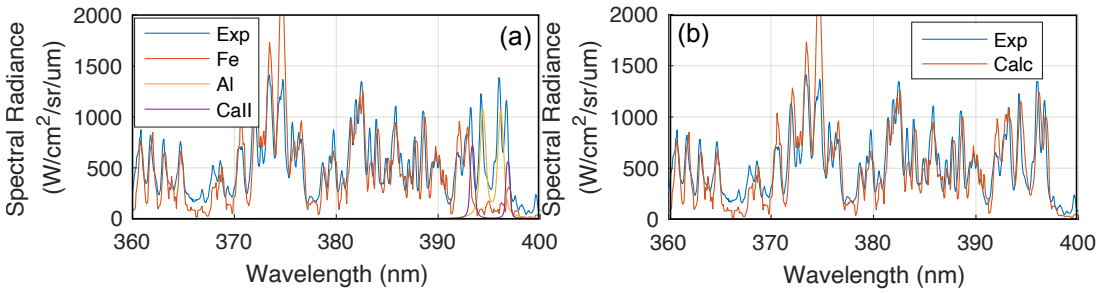

Figure 11: Example spectra from test 5011 (aluminium) compared with modelled spectra for atomic contaminants. (a) Individual intensities for each species; (b) Summed intensities from all modelled species.

The figure shows that vast majority of the spectral lines can be identified as due to the presence of iron in the flow, although spectral lines of aluminium and ionised calcium are also observed. The right plot in the figure shows the sum of all the calculated spectra overlaid with the experimental measurements. The observed fit is generally good for most lines, particularly noting that these are absolute comparisons. The inferred temperature from the fitting process is around 5,200 K, consistent with numerical simulations of the flow [4].

Figure 12 shows comparative spectra for three different tests: unheated carbon-carbon, unheated aluminium and heated graphite. Three plots are shown corresponding to the shock layer, viscous layer and expansion region (noting that the scale of the latter is ten times smaller than the others). All three spectra show similar features, with almost all spectral lines identified as being due to iron. The test with an aluminium plate shows higher levels of iron, possibly due to shot-to-shot variation in the levels of contamination. We can conclude from these tests that there is no evidence of any ablation from any of these inserted plates having any impact on the observed flow species in any region downstream of the plate.

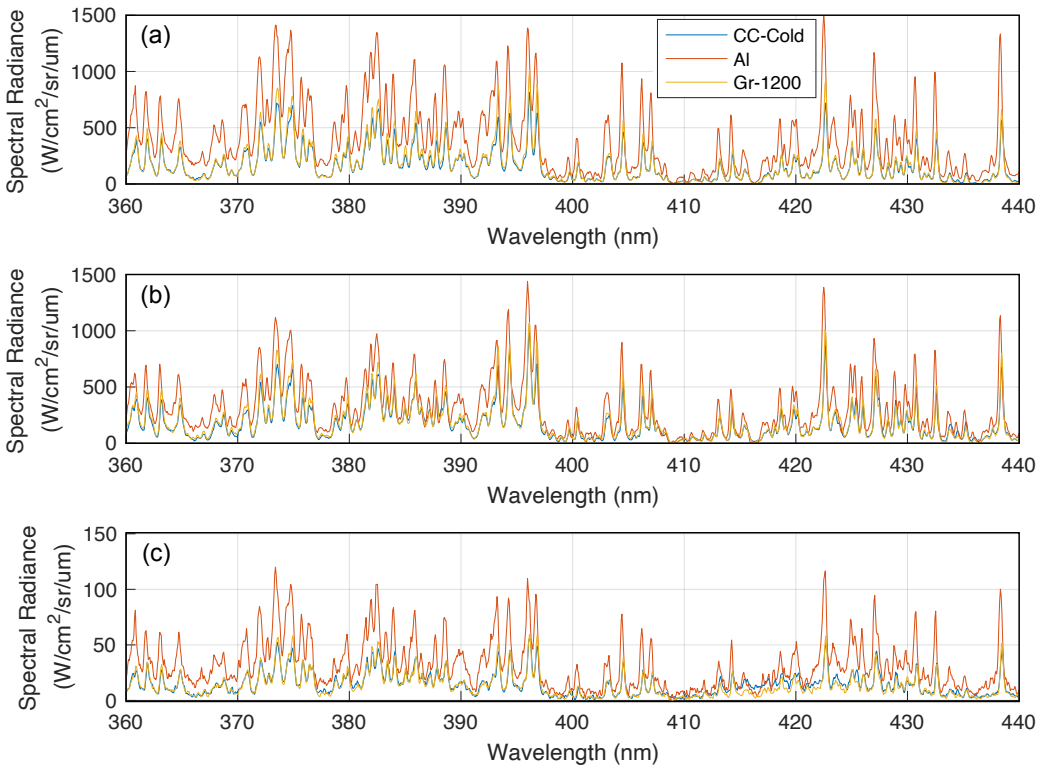

Figure 12: Example spectra from tests 5011 (aluminium), 5020 (cold C-C), 5031 (heated graphite). (a) Shock layer; (b) Viscous layer; (c) Expansion region.

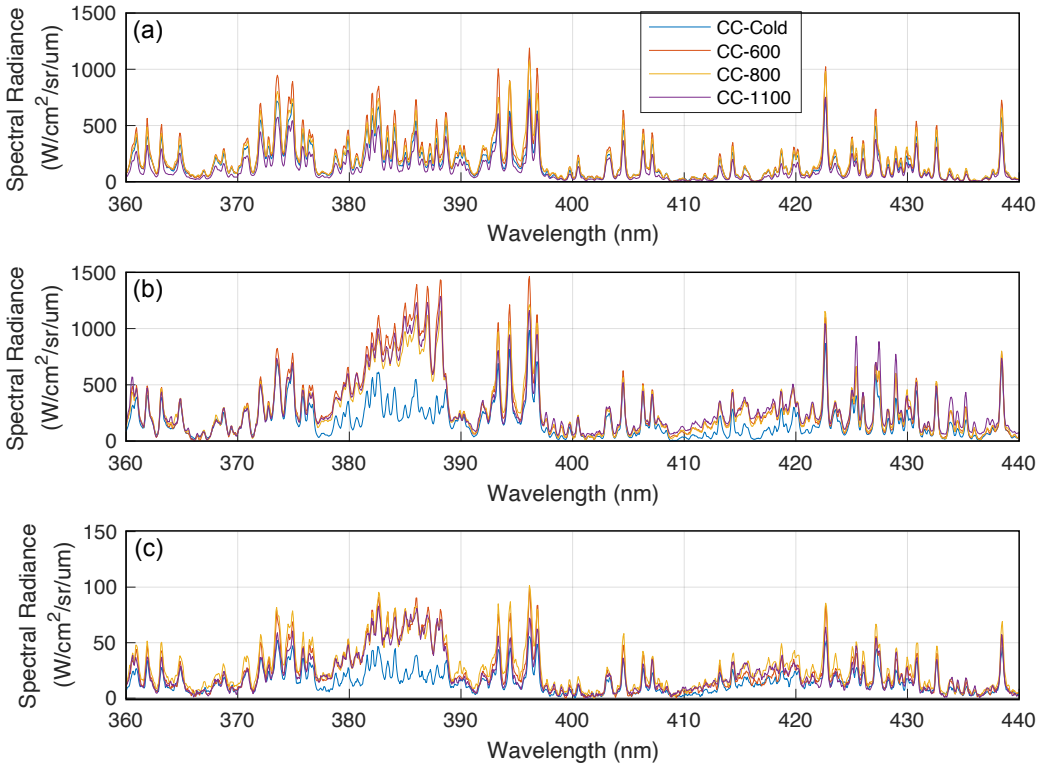

Figure 13: Example spectra from C-C tests 5020 (Cold), 5033 (600 A), 5032 (800 A), 5034 (1100 A). (a) Shock layer; (b) Viscous layer; (c) Expansion region.

The tests using a heated carbon-carbon insert, shown in Fig. 13, in contrast, provide clear evidence of species ablated from the plate entering the flow. The spectra in the shock layer in this figure show little difference between the tests with different heating levels, but both the viscous layer and the expansion region show spectra bands due to the CN molecule. These bands are most evident in the wavelength range 380-390 nm (CN violet, $\Delta v = 0$) but there is also evidence of differences over the range 410-420 nm (CN violet, $\Delta v = -1$), particularly in the viscous layer. It can be concluded that ablative products from the heated plates (presumably carbon or carbon compounds) enter the flow leading to chemical reactions with nitrogen in the test gas forming CN. Interestingly, these reactions seem to be saturated for all levels of heating investigated here, with the levels of radiation observed seemingly independent of the heating level.

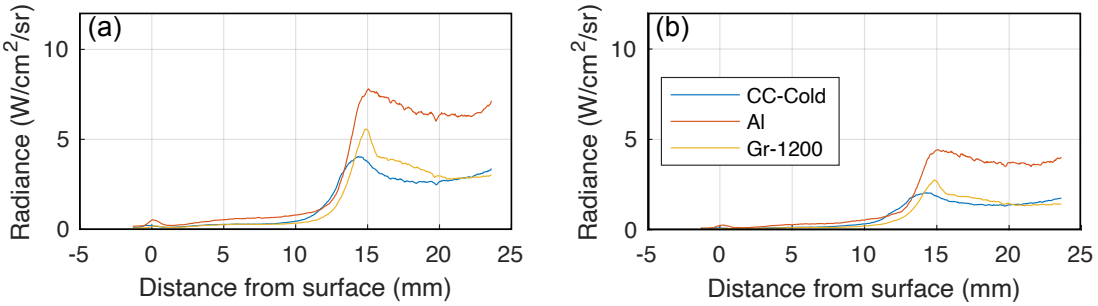

Figure 14: Spatial variation in radiance from tests 5011 (aluminium), 5020 (cold C-C), 5031 (heated graphite). (a) Calculated over wavelengths 380-390 nm (CN band); (b) Calculated over wavelengths 400-410 nm.

The spatial distribution of the radiating species can be investigated by calculating the radiance over given wavelength ranges. Such a calculation is shown in Fig. 14 for the unheated carbon-carbon, unheated aluminium, and heated graphite (corresponding to spectra in Fig. 12). Fig. 14(a) shows the radiance over wavelengths 380-390 nm (the wavelength range where CN is observed in the hot C-C tests), while Fig. 14(b) shows radiance over the wavelength range 400-410 nm (no radiating CN). For these tests, both plots show similar trends in that elevated radiances in the shock layer are reflected in elevated levels in the viscous layer and the expansion region. We can conclude that all spectral lines originate from contaminants which were present within the free-stream and have similar relative concentrations in the viscous layer and expansion region.

Fig. 15 shows similar plots for the carbon-carbon tests. As was previously observed,

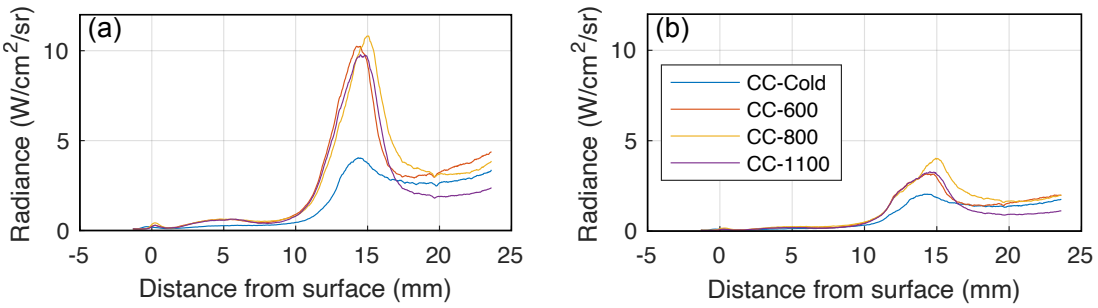

Figure 15: Spatial variation in radiance from C-C tests 5020 (Cold), 5033 (600 A), 5032 (800 A), 5034 (1100 A). (a) Calculated over wavelengths 380-390 nm (CN band); (b) Calculated over wavelengths 400-410 nm.

there are elevated levels of CN within the viscous layer and the expansion region for heated C-C tests, and this is reflected in the higher radiances in the wavelength range 380-390 nm. There is also some evidence of slightly elevated levels of radiation at other wavelengths (including 400-410 nm) and this will require further investigation.

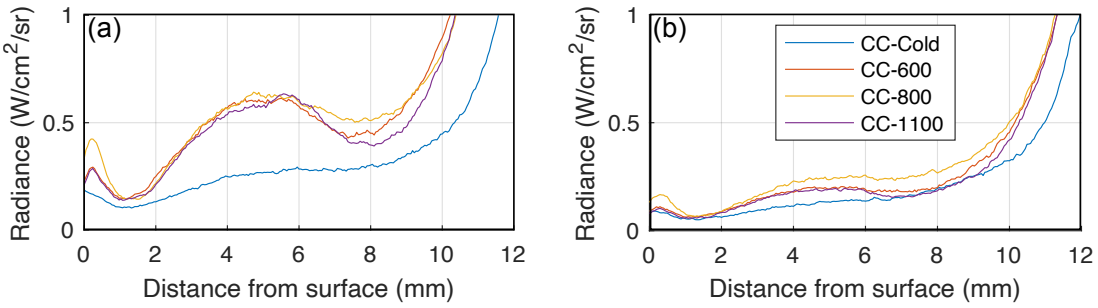

Figure 16: Expansion region spatial variation in radiance from C-C tests 5020 (Cold), 5033 (600 A), 5032 (800 A), 5034 (1100 A). (a) Calculated over wavelengths 380-390 nm (CN band); (b) Calculated over wavelengths 400-410 nm.

Of particular interest is the impact of ablated products on the flow within the expansion region behind the step. Fig. 16 shows an enlarged view of this region. The radiance levels for the heated carbon-carbon tests are observed to peak at the centre of this region (5 mm above the surface). A small region of elevated radiance is also observed near the body. These spectra confirm that the ablation process for a heated carbon-carbon plate does impact on the radiation levels observed in the expansion region in these tests.

4.4 Outlook

The experiments in this study have been successful in producing some of the first experimental measurements of radiation in the wake region of a test model with a heated surface. The measurements conducted with the second test model were especially successful in that good resolution spectra were recorded. These measurements form a key database that can be used for comparison with numerical simulations of such flows. Ongoing work can be divided into two aspects: further analysis of the current study, and future experimental and numerical studies. Some key aspects are discussed below.

Further analysis of the current experimental measurements continues:

- The spectral analysis for the single compression model has thus far concentrated on the spectral region 360-440 nm in which radiation from the CN molecule is known to occur. Measurements were also taken at higher wavelengths (445-525 nm) and in the infra-red. These spectra will be analysed to investigate for any other differences between cold and hot testing.
- Shot-to-shot repeatability will be further investigated by comparing other repeat tests with those already analysed.
- Modelling of the spectra of the contaminant species has been developed as part of this project, and detailed comparisons between such spectra and the experimental data will also be continued.

- Numerical simulations by developed by AFIT and by UQ will continue. It will be of particular interest to make comparisons with the measurements in the expanding region of the flow.

Future experimental studies are planned:

- Further investigation of the impact of varying the surface temperature of the plate (in particular lower temperatures than in the current study) should be conducted to identify the threshold for which ablative processes impact the downstream flow radiation.
- Measurements could also be performed using filtered imaging to obtain two-dimensional images of the radiating flow restricted to wavelengths over which CN or other species radiate.
- Spectroscopic measurements at other wavelengths should be conducted. It could be beneficial to identify the presence of atomic carbon (and/or other carbon based molecules such as CO) in the flow. This may necessitate measurements in the vacuum ultraviolet region of the spectrum (previously achieved in X2) and/or at infrared wavelengths.
- Studies should be conducted using different operating conditions. The current study focussed on one flow enthalpy, but outcomes may vary at higher or lower enthalpies.
- Measurements should be conducted with an axisymmetric model. Such a configuration may be more difficult experimentally, both in constructing a model with a heated surface as well as analysing the spectra. Nevertheless, such an approach eliminates any issues with edge effects that occur for two-dimensional wedge configurations.
- Double compressions or other configurations could be further studied once a better modelling capability of simpler configurations is achieved.

References

[1] Gildfind, D.E., *Development of High Total Pressure Scramjet Flow Conditions using the X2 Expansion Tube*, Ph.D. Dissertation, Centre for Hypersonics, The University of Queensland, 2012.

[2] Zander, F., *Hot Wall Testing in Hypersonic Impulse Facilities*, Ph.D. Dissertation, Centre for Hypersonics, The University of Queensland, 2013.

[3] Temme, N., *Hypervelocity boundary-layer flow experiments with high surface temperature ablation*, Ph.D. Dissertation, Centre for Hypersonics, The University of Queensland, 2021 (submitted).

[4] MacDermott, R., Greendyke, R., Temme, N., Morgan, R., and McIntyre, T., *Experimental Analysis of Hypersonic Carbon-Carbon Ablation in Representative-Wake Expansion Regions*, JANNAF Journal of Propulsion and Energetics, Vol 12, Issue 1, 2021.

Appendix

The following table lists the details of all tests conducted during the campaign.
Heating: peak temperature (or current)
View: high-speed imaging directions
Compression/Expansion: location of spectroscopic measurements
High/low: resolution of spectroscopic measurements

Table 4: All campaign tests - Part 1

Test	Shot	Model	Plate	Heating	View	Compression	Expansion	Expansion
1	4584	Double	C-C	1000 K	Side	350 nm/low	-	-
2	4585	Double	C-C	1300 K	Side	350 nm/low	-	-
3	4586	Double	C-C	1100 K	Side	350 nm/low	-	-
4	4587	Double	C-C	1470 K	Side	350 nm/low	-	-
5	4588	Double	C-C	1560 K	Side	350 nm/low	-	-
6	4589	Double	C-C	1000 K	Side	550 nm/low	-	-
7	4590	Double	C-C	Cold	Side	550 nm/low	-	-
8	4591	Double	C-C	Cold	Side	350 nm/low	-	-
9	4592	Double	C-C	Cold	Side	750 nm/low	-	-
10	4593	Double	C-C	1200 K	Side	750 nm/low	-	-
11	4594	Double	C-C	2000 K	Side	750 nm/low	350 nm/low	-
12	4595	Double	Al	Cold	Side	350 nm/low	350 nm/low	-
13	4596	Double	Al	Cold	Side/top	550 nm/low	350 nm/low	-
14	4597	Double	Al	Cold	Side/top	750 nm/low	350 nm/low	-
15	4598	Double	Al	Cold	Side/top	750 nm/low	350 nm/low	-
16	4599	Double	Al	Cold	Side/top	750 nm/low	350 nm/low	-
17	4600	Double	Al	Cold	Side/top	350 nm/low	350 nm/low	-
18	4601	Double	Al	Cold	Side/top	550 nm/low	550 nm/low	-
19	4602	Double	C-C	2000 K	Side	550 nm/low	550 nm/low	-
20	4603	Double	C-C	2300 K	Side	350 nm/low	350 nm/low	-
21	4604	Double	C-C	1500 K	Side	350 nm/low	350 nm/low	-
22	4605	Double	Gr.	1500 K	Side	350 nm/low	350 nm/low	-
23	4990	Double	Al	Cold	Side	350 nm/high	350 nm/high	-
24	4991	Double	Al	Cold	Side/top	350 nm/high	350 nm/high	-
25	4992	Double	Al	Cold	Side/top	350 nm/high	350 nm/high	-
26	4993	Double	Al	Cold	Side/top	550 nm/high	550 nm/high	-
27	4994	Double	Al	Cold	Side/top	550 nm/high	550 nm/high	-
28	4995	Double	Al	Cold	Side/top	550 nm/high	550 nm/high	-
29	4996	Double	Al	Cold	Side/top	750 nm/high	750 nm/high	-
30	4997	Double	Al	Cold	Side/top	750 nm/high	750 nm/high	-
31	4998	Double	Gr.	Cold	Side/top	400 nm/high	400 nm/high	-
32	4999	Double	Gr.	Cold	Side/top	400 nm/high	400 nm/high	-
33	5000	Double	Gr.	Cold	Side/top	485 nm/high	485 nm/high	-
34	5001	Double	Gr.	Cold	Side/top	485 nm/high	485 nm/high	-

Table 5: All campaign tests - Part 2

Test	Shot	Model	Plate	Heating	View	Compression	Expansion	Expansion
35	5002	Single	C-C	Cold	Side/top	400 nm/high	400 nm/high	-
36	5003	Single	C-C	Cold	Side/top	400 nm/high	400 nm/high	-
37	5004	Single	C-C	Cold	Side/top	400 nm/high	400 nm/high	-
38	5005	Single	C-C	Cold	Side/top	485 nm/high	485 nm/high	-
39	5006	Single	C-C	Cold	Side/top	485 nm/high	485 nm/high	-
40	5007	Single	Al	Cold	Side/top	485 nm/high	485 nm/high	-
41	5008	Single	Al	Cold	Side/top	485 nm/high	485 nm/high	-
42	5009	Single	Al	Cold	Side/top	400 nm/high	400 nm/high	-
43	5010	Single	Al	Cold	Side/top	400 nm/high	400 nm/high	-
44	5011	Single	Al	Cold	Side/top	400 nm/high	400 nm/high	2250nm/high
45	5012	Single	Al	Cold	Side/top	-	400 nm/high	2250nm/high
46	5013	Single	Al	Cold	Side/top	-	485 nm/high	2250nm/high
47	5014	Single	Gr.	Cold	Side/top	-	485 nm/high	2250nm/high
48	5015	Single	Gr.	Cold	Side/top	-	485 nm/high	2250nm/high
49	5016	Single	Gr.	(700 A)	Side/top	-	485 nm/high	2250nm/high
50	5017	Single	Gr.	(700 A)	Side/top	485 nm/high	485 nm/high	1550nm/high
51	5018	Single	Gr.	(700 A)	Side/top	400 nm/high	400 nm/high	1550nm/low
52	5019	Single	C-C	(1000 A)	Side/top	400 nm/high	400 nm/high	1550nm/low
53	5020	Single	C-C	Cold	Side/top	400 nm/high	400 nm/high	1550nm/low
54	5021	Single	C-C	(1000 A)	Side/top	400 nm/high	400 nm/high	1550nm/low
55	5022	Single	C-C	(1000 A)	Side/top	400 nm/high	400 nm/high	1550nm/low
56	5023	Single	C-C	(1000 A)	Side/top	485 nm/high	485 nm/high	1550nm/low
57	5024	Single	C-C	Cold	Side/top	485 nm/high	485 nm/high	1550nm/low
58	5025	Single	C-C	Cold	Side/top	485 nm/high	485 nm/high	1550nm/low
59	5026	Single	C-C	(600 A)	Side/top	485 nm/high	485 nm/high	1550nm/low
60	5027	Single	Gr.	1200 K	Side/top	485 nm/high	485 nm/high	1550nm/low
61	5028	Single	Gr.	1400 K	Side/top	485 nm/high	485 nm/high	1550nm/low
62	5029	Single	Gr.	Cold	Side/top	400 nm/high	400 nm/high	1550nm/low
63	5030	Single	Gr.	(800 A)	Side/top	400 nm/high	400 nm/high	1550nm/low
64	5031	Single	Gr.	2300 K	Side/top	400 nm/high	400 nm/high	1550nm/low
65	5032	Single	C-C	2000 K	Side/top	400 nm/high	400 nm/high	1550nm/low
66	5033	Single	C-C	1700 K	Side/top	400 nm/high	400 nm/high	1550nm/low
67	5034	Single	C-C	2200 K	Side/top	400 nm/high	400 nm/high	1550nm/low
68	5035	Single	C-C	(700 A)	Side/top	400 nm/high	400 nm/high	1550nm/low
69	5036	Single	C-C	(1000 A)	Side/top	400 nm/high	400 nm/high	1550nm/low
70	5037	Single	Al	Cold	Side/top	400 nm/high	400 nm/high	1550nm/low